

Optical Sensing for the HEDS-1000

Introduction

The rapid growth of the digital processing used in commercial, industrial and consumer products, has created the need for sensors that convert physical parameters into electrical signals which may directly interface to a digital system. Optical sensors have utility in each of these areas, in that they provide a quick non-contact response to the parameters sought as a data source. Commercial applications include bar code scanning, paper edge sensing, end of tape sensing, and position and magnetic tape loop stabilizing. Industrial uses may consist of optical tachometry, assembly line monitoring, and safety interlocks, while the consumer uses of the optical sensor may be found in audio products, entertainment products, and video games.

This application note describes the electrical and optical design considerations for using discrete optoelectronic devices, or the HEDS-1000 High Resolution Optical Reflective Sensor. The application areas addressed include non-contact transmissive, or reflective sensor systems.

Each of these application areas includes an optical emitter, a transmission path, and a detector to perform the sensing function. The sensing may occur by having the object obstruct the transmission path, or complete it by reflecting the emitter beam to the detector. In either the transmissive or reflective sensing configuration, there are optical, electrical, and mechanical considerations that must be addressed in order to insure optimum performance of the emitter/detector system.

System Elements

Every optical sensor system includes a source of optical flux, a transmission path, and a receiving detector. In most sensor system analysis, the available flux and the responsivity of the receiver are considered to be constant and consequently the dynamic incidence change found at the receiver results from modifications of the transmission path. Figure 1 shows a paper tape reader and densitometer examples of transmissive sensor systems. The presence or absence of the paper hole results in a binary

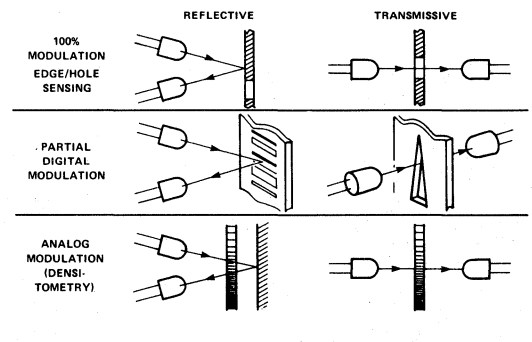


Figure 1. Different Techniques of Flux Path Modulation.

ON-OFF transmission path attenuation. The densitometer functions by causing an analog modulation of the transmission path. Bar code scanning and paper edge sensing are applications of reflective sensor techniques shown in Figure 1. The bar code provides a reflective contrast between the background and the bars. It is the reflective differential that modulates the transmission path. In paper edge sensing applications, the paper edge creates a digital responding transmission system. When the paper edge is not present in the reflecting field of the sensor, the flux transmission will be zero, and the transmittance will increase when the edge is in the field.

Optical Transfer Function

The characteristics of the transmission path can be estimated through the use of an optical transfer function, OTF. The function is the ratio of the total optical flux available, ϕ_e , to the incident flux arriving at the receiver, $\phi_e(R)$. This function allows the designer to calculate the amount of photocurrent available for the detector amplifier.

$$OTF = \frac{\phi_e(\text{RECEIVED})}{\phi_e(\text{AVAILABLE})} \quad (1)$$

The optical flux attenuation comes from a number of causes. One cause is the transmission loss as the flux is incident upon and passes through the transmission media. These losses come about because of reflection at the surface of the material, and scattering and absorption within the material. For the calculation of the optical transfer function, it is customary to describe these losses, τ , in terms of a transmittance, T , of the material for the wavelength of the source. The transmittance is equal to:

$$T = (1 - \tau) \quad (2)$$

Another cause of attenuation is the incomplete coupling of the flux from the source to the receiver caused by the mismatch of the receiver relative aperture to the source relative aperture.

Coupling Fundamentals

The general case of source flux coupled to a receiver is dependent upon the source radiation pattern, the source-receiver spacing, and the receiver area. The following analyses show how these parameters affect the OTF.

Figure 2 shows a source which is located at the center of a hemisphere with a receiver of an area A located at a distance, d , from the apex. The ratio of the receiver area to the distance squared defines the solid angle, ω , sub-

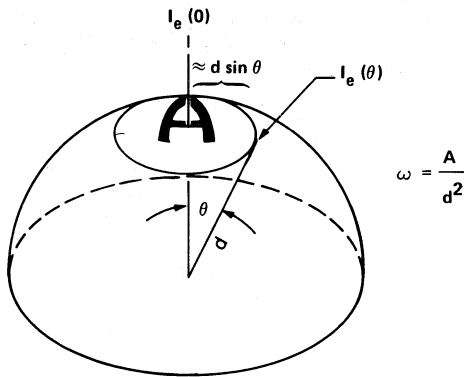


Figure 2. Definition of the Solid Angle, ω .

tended by the area, A . The total flux, ϕ_e , being radiated is the integral of the flux incident within the hemisphere. The radiation pattern of a Lambertian source is shown in Figure 3. The pattern describes the ratio of the radiant intensity at an off-axis angle, $I_e(\theta)$ to the axial radiant intensity, $I_e(0)$. The radiation pattern for a Lambertian source (or the reception pattern for a Lambertian receiver) is described by the cosine of the off-axis angle. The Lambertian radiation pattern function is:

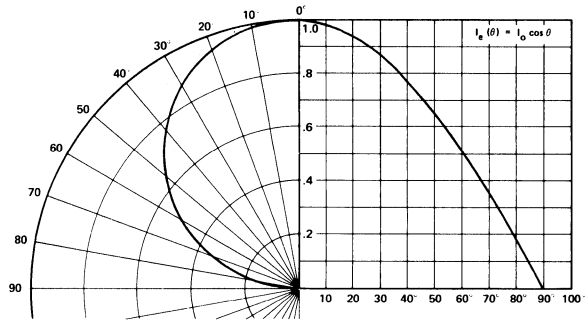


Figure 3. Radiation Pattern of a Lambertian Source.

$$I_e(\theta) = I_e(0) \cos \theta \quad (3)$$

When the radiation pattern, $I_e(\theta)/I_e(0)$, and the axial radiant intensity, $I_e(0)$, are known, Equation (4) can be used to determine the total flux into the hemisphere, ($\theta = 90^\circ$) or the flux into a cone created by the area, A .

$$\phi_e(\theta) = I_e(0) \int_0^\theta \frac{I_e(\theta)}{I_e(0)} 2\pi \sin \theta d\theta \quad (4)$$

When a Lambertian radiator is used as a source, the flux into the cone specified by the off-axis angle, θ , is calculated from Equations (3) and (4).

$$\phi_e(\theta) = I_e(0) \int_0^\theta 2\pi \cos \theta \sin \theta d\theta$$

$$\phi_e(\theta) = I_e(0) \pi \sin^2 \theta \quad (5)$$

The total flux, ϕ_e , of the Lambertian source is obtained from Equation (5) when $\theta = 90^\circ$. Thus, the total flux ϕ_e is π times the axial radiant intensity, $I_e(0)$.

The amount of flux coupled into the receiver area A relates to the relative aperture of the receiver. The relative aperture, also known as the numerical aperture, N.A., defines the ability of the receiver to accept flux arriving at off-axis angles. When a source with a specific radiation pattern is considered, a receiver with a large numerical aperture will capture more flux than one with a smaller N.A. The numerical aperture is defined as the sine of one-half the included angle of the receiver cone. Thus,

$$N.A. = \sin \theta \quad (6)$$

where $\theta = \frac{1}{2}$ cone angle.

As seen in Figure 4, when small angles of θ are considered, the numerical aperture can be calculated as:

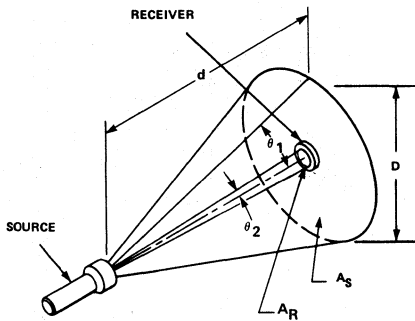


Figure 4. Illustration of Numerical Aperture Relationships.

$$N.A. = \sin \theta \approx D/2d$$

$$N.A. = \sin \theta \approx (A/\pi)^{1/2}/d$$

$$N.A.^2 = \sin^2 \theta \approx A/\pi d^2 \quad (7)$$

In Figure 4 are shown a source and a receiver separated by a distance, d . At that distance, the cone (θ_1) of radiation from the source irradiates an area, A_S . Clearly, the receiver having an area, A_R , much smaller than A_S , describes a smaller cone (θ_2) and will receive only a fraction of the flux radiated by the source. This fraction describes the Optical Transfer Function (OTF) for this simple situation, and a good estimate of the value of this fraction is the ratio of the areas A_R/A_S . Then, applying the relationship derived in Equation (7), the OTF can be defined in terms of the cones for source and receiver which are described by numerical apertures:

$$\begin{aligned} OTF &= \frac{\phi_R}{\phi_S} = \frac{A_R}{A_S} = \frac{\pi d^2 N.A._R^2}{\pi d^2 N.A._S^2} \quad (8) \\ &= \left(\frac{N.A._R}{N.A._S} \right)^2 = \left(\frac{\sin \theta_2}{\sin \theta_1} \right)^2 \end{aligned}$$

In estimating OTF, it is necessary only to recognize and evaluate such cones of coupling — exit cone (or N.A.) and acceptance cones. As a general rule, the cone angle, θ , is defined as the angle at which coupling is 0.1 (10%) of the axial value ($\theta = 0$). A case of special interest is that of a Lambertian emitter having a radiation pattern varying as $\cos \theta$. The angle at which $\cos \theta = 0.1$ is 84.26° , at which $\sin \theta = N.A. = 0.995$; thus, for practical purposes, a Lambertian source is regarded as having $N.A. = 1$. If, in Figure 4, a Lambertian source were used, the relationship in Equation (8) reduces:

$$OTF = \left(\frac{N.A._R}{N.A._S} \right)^2 = \left(\frac{N.A._R}{1} \right)^2 = (N.A._R)^2 \quad (9)$$

This simplification is important as it is used extensively in the sections to follow. Notice, however, that OTF cannot

exceed unity, so that if $N.A._R > N.A._S$, then $OTF = 1$. This occurs when the acceptance cone of the receiver is larger than the exit cone of the source.

Lens Fundamentals

In practical sensor applications, the source-receiver distance might be ten or more times the diameter of the receiver. If the receiver area is small relative to d , then by Equation (7), the receiver numerical aperture will be small. If the source is Lambertian, the total flux coupling will then relate to the square of this small numerical aperture.

Through the use of lens, more efficient coupling will result. In order to understand how this is accomplished, it is helpful to present a few rules of optics. The first is the basic lens equation. Referring to Figure 5 a double convex condensing lens is shown relaying an image from the source to the receiver. The source is located a distance, d_S , from the lens and the real image is located at a distance, d_R , which is related to the focal length of the lens. Thus, the relationship of d_S , d_R , f is called the basic lens equation.

$$\frac{1}{f} = \frac{1}{d_S} + \frac{1}{d_R} \quad (10)$$

where f = Focal Length

d_S = Source Lens Distance

d_R = Received Image Distance

This relay lens system is focused when the receiver is placed at the distance, d_R , [from Equation (10) when f and d_S are known] from the lens.

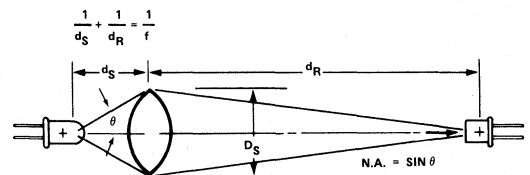
Under the focused condition, the image of the source (at the plane of the receiver) is magnified. The degree of magnification, m , is equal to the ratio of d_R to d_S .

$$m = \frac{d_R}{d_S} \quad (11)$$

$$m^2 = \frac{A_{S,M}}{A_S} \quad (12)$$

where $A_{S,M}$ = Source Image (Source Magnified)

A_S = Source Area



OTF = $N.A._L^2 \cdot T$, FOR A LAMBERTIAN SOURCE WITH IMAGE AREA SMALLER THAN RECEIVER AREA

Figure 5. Focused Emitter Detector System Using a Double Convex Lens.

Using Equations (10) and (11), the magnification can be represented in terms of the focal length and source to lens distance, d_S .

$$A_{S,M} = m^2 A_S = \left(\frac{f}{d_S - f} \right)^2 \cdot A_S \quad (13)$$

When the source-lens distance, d_S , is twice the focal length, f , the image will appear at $d_R = 2f$ on the other side of the lens. Under a $2f$ focused condition, the area of the image $A_{S,M}$, is equal to the area of the source A_S . This configuration is termed a 1:1 magnification or $2f$ system.

Lenses also have relative aperture qualities. The relative aperture may be specified as either a numerical aperture, N.A., or as an f -number, $f/$. The f -number is equal to the ratio of the focal length to the diameter of the lens. The f -number and the numerical aperture are inversely related, such that a smaller f -number will result in a proportionately larger N.A.

In Figure 5, the effective diameter of the lens is D_L , and relative to this, the numerical aperture is approximately $D_L/2d_S$ as in Equation (7). Comparing the definitions of $f/$ no and N.A.:

$$\begin{aligned} f/\text{no} &= \frac{f}{D_L} & \text{N.A.} &\approx \frac{D_L}{2d_S} \\ f/\text{no} &= \frac{1}{2\text{N.A.}} \left(\frac{f}{d_S} \right) \end{aligned} \quad (14)$$

When $d_S = f$, the source is focused at infinity, making $\text{N.A.} = 1/2(f/\text{no})$; when $d_S < f$, there is no real image, but a virtual image of the source lying on the same side of the lens, and the lens is less effective in improving the coupling.

Lens Coupling

The amount of flux coupled into the lens is dependent upon the numerical aperture of the lens and the exit aperture of the source. When a focused lens system is considered such as that shown in Figure 5, the flux that arrives at the received image point is equal to the ratio of the square of the numerical aperture of the lens divided by the square of the exit numerical aperture of the source, this total times the transmittance, T , of the lens. Thus, the lensed OTF is equal to:

$$\text{OTF} = \frac{\phi_R}{\phi_S} = \left[\frac{\text{N.A.}_L}{\text{N.A.}_S} \right]^2 \cdot T \quad (15)$$

When the source is Lambertian, the equation simplifies to:

$$\text{OTF} = \frac{\phi_R}{\phi_S} = \text{N.A.}_L^2 \cdot T \quad (16)$$

The following will illustrate a practical example:

Given: Detector Area $A_D = .1 \text{ mm}^2$
 Lambertian Source $A_S = .1 \text{ mm}^2$, $\phi_S = 100 \mu\text{W}$
 Lens Numerical Aperture $\text{N.A.}_L = .5$
 Lens Focal Length, $f = 5 \text{ mm}$
 Lens Transmittance, $T = .95$
 Lens to Source Distance, $d_S = 20 \text{ mm}$
 Lens to Receiver Distance, $d_R = 6.67 \text{ mm}$

Using Equation (15), the flux at the receiver will be:

$$\phi_R = \phi_S \text{N.A.}_L^2 \cdot T \quad (17)$$

$$\phi_R = 100 \mu\text{W} (.5)^2 \cdot .95$$

$$\phi_R = 23.75 \mu\text{W}$$

The received area is determined by Equation (12).

$$A_{S,M} = \left(\frac{f}{d_S - f} \right)^2 \cdot A_S \quad (18)$$

$$A_{S,M} = \left(\frac{5 \text{ mm}}{20 \text{ mm} - 5 \text{ mm}} \right)^2 \cdot .1 \text{ mm}^2 = .011 \text{ mm}^2$$

Thus, into an area of $.011 \text{ mm}^2$, a flux of $23.75 \mu\text{W}$ is concentrated. Using the basic lens equation, (10), the received image lies 6.7 mm from the lens. If a photodiode with an area, A_D , were placed at this distance, d_R , the fraction of this flux that couples the detector is the ratio of A_D to $A_{S,M}$ if the detector area lies entirely within the source image area. In general, this fraction is the ratio of that portion of the source image that overlaps the receiver, divided by the total source image area, and therefore cannot exceed unity, even when the detector area A_D is much larger than the source image area, $A_{S,M}$.

$$\text{Detector Coupling} = K_D = \frac{A_D}{A_R} \leq 1 \quad (19)$$

When a lens coupling is compared with non-lens coupling, the improvement is described by:

$$\frac{\phi_L}{\phi_{n-L}} = \frac{\text{N.A.}_L^2 \cdot T}{\text{N.A.}_R^2} ; \text{N.A.}_R^2 = A_D / [\pi (d_S + d_R)^2]$$

where N.A._R is found from Equation (7) with $d = d_S + d_R$

$$\frac{\phi_L}{\phi_{n-L}} = \frac{(.5)^2 \cdot .95}{4.47 \times 10^{-5}} = 5.3 \times 10^3$$

Thus, this simple example using a lens improves the coupling gain by 37dB.

Reflector Fundamentals

Sensor applications, such as bar code scanning, paper edge detection, and optical tachometry, use the reflective properties of the object or element that they sense.

The reflection of the incident flux may either be specular or diffuse. A specular reflector is one where the angle of the reflected ray of flux is equal to the incident ray of flux. Thus, if a ray of flux was incident to the reflector at 20° from the normal, the reflected ray would also be 20° from the normal and 40° from the incident. A first surface mirror or a highly polished code wheel are examples of specular reflectors. They are characterized as having reflection coefficients, ρ , of almost unity. It has a numerical aperture, $N.A.R-S$, equal to the $N.A.$ of the source that is incident upon it. The reflected flux would be equal to incident flux times the reflection coefficient.

$$\phi_{OUT} = \phi_{IN} \frac{N.A.L^2}{N.A.R-S^2} \cdot \rho; \text{ where } N.A.R-S = N.A.L$$

$$\phi_{OUT} = \phi_{IN} \rho \quad (20)$$

The reflection coefficient is assumed to be constant over the wavelengths of interest. If this is not true, then a correction coefficient, $k\rho(\lambda)$ must be introduced to correct for this spectral property.

A perfectly diffuse reflector is characterized as having a Lambertian radiation pattern. The flux that is coupled from the reflector is equal to:

$$\frac{\phi_{OUT}}{\phi_{IN}} = \frac{N.A.RECEIVER^2}{N.A.REFLECTOR^2} \cdot \rho \quad (21)$$

In typical applications, the numerical aperture of the receiver will be that of the receiving lens. Also, the $N.A.$ of the diffuse surface is unity; therefore, Equation (21) can be rewritten as:

$$\frac{\phi_{OUT}}{\phi_{IN}} = N.A.L^2 \cdot \rho \quad (22)$$

Most reflectors are neither perfectly specular or diffuse, but a combination of the two. A typical diffuse reflector may appear more specular at one wavelength and more diffuse at another. Also, the angle of incidence may modify the reflection properties.

It may be desirable in reflective sensor applications to compute the relative ratio of reflection between a specular and a diffuse reflector. Assuming both applications have the same ϕ_{IN} and the same receiving lens, and using Equations (20) and (21), this ratio becomes:

$$\frac{\phi_{OUT} (SPECULAR)}{\phi_{OUT} (DIFFUSE)} = \frac{\rho_S}{N.A.L^2 \rho_D} \quad (23)$$

Thus, if the receiving lens had a $N.A.L = .3$, the effective gain of using a specular over a diffuse reflector would be 10.45dB.

Confocal Coupling

It was shown in the lens coupling section that the area of the source could be reduced or magnified through the use of a lens. The technique of reducing the image of the receiver and the source, such that they lie on the same plane located a distance between the source and sensor can be accomplished by using two confocally spaced pair of lenses.

Figure 6 shows two plano-convex lenses positioned so that they are confocally focused. Using the coupling concept developed in the coupling fundamentals the overall OTF can be developed in the following steps.

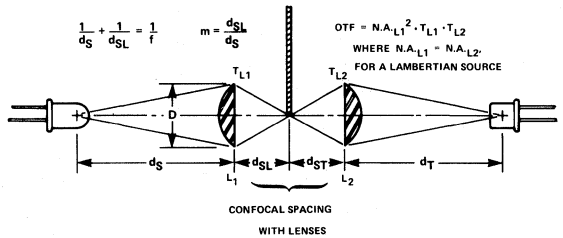


Figure 6. Confocal Spaced Emitter Detector System Employing Two Plano Convex Lenses.

Step 1. Flux into Lens 1.

$$\frac{\phi_{L1}}{\phi_S} = \frac{\text{entrance } N.A.L1^2}{N.A.S^2} \cdot T_{L1} \quad (24)$$

Step 2. Flux into Lens 2 from Lens 1.

$$\frac{\phi_{L2}}{\phi_{L1}} = \frac{\text{entrance } N.A.L2^2}{\text{exit } N.A.L1^2} \quad (25)$$

Step 3. Total OTF.

$$OTF = \frac{\phi_{L2}}{\phi_S} \quad (26)$$

$$= \frac{\text{entrance } N.A.L1^2}{\text{exit } N.A.S^2} \cdot \frac{\text{entrance } N.A.L2^2}{\text{exit } N.A.L1^2} \cdot T_{L1} \cdot T_{L2}$$

The convenient fact about such a transfer function is that each element of the linear system can be evaluated and then the total function is the product of the individual terms.

In a practical application, the exit $N.A.$ of lens 1 and the entrance $N.A.$ of lens 2 will be equal. If a Lambertian

source were used in Equation (24), it would reduce to $N.A._{L1}^2 T_{L1}$. These two conditions allow the following.

$$\text{Confocal OTF} = \frac{\phi_{L2}}{\phi_S} = N.A._{L1}^2 \cdot T_{L1} \cdot T_{L2} \quad (27)$$

The image size appearing equidistant between the two lens surfaces is determined by the magnification factor, $m = d_{SL}/d_S$. Thus, a large source and receiver can be focused down to a point in space, and when confocally coupled, the imaged source-receiver area can become the interruption point for a hole edge, or paper edge sensor.

Lens Reflective Coupling

If one of the lenses of a confocally coupled lens system were placed adjacent to the other lens element and skewed so that the two images in front of the lenses intersected, a lensed reflective sensor would result. This is shown in Figure 7.

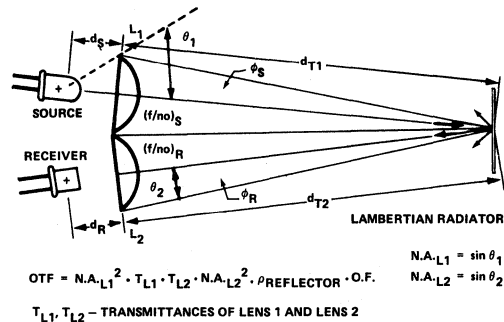


Figure 7. Reflective Coupling Employing Confocally Spaced Lenses.

Every mechanical system has alignment tolerances which may allow the two images at the focused point to move with respect to one another so that the area of the source and receiver images do not totally overlap. The ratio of the image overlap is termed the overlap fraction, OF.

$$O.F. = \frac{\left(\frac{\text{AREA OF SOURCE IMAGE WHICH IS OVERLAPPED BY RECEIVER IMAGE}}{\text{TOTAL AREA OF SOURCE IMAGE}} \right)}{\leq 1} \quad (28)$$

This fraction can vary from zero to unity. When it is zero, no coupling occurs and at unity, maximum coupling results. If the receiver image overlaps the entire source image, the O.F. will have its maximum value of unity. Having a larger receiver image provides a more consistent O.F. by reducing variability due to alignment difficulty.

The amount of flux coupling would be dependent upon the type and reflectance of the reflector placed at the image intersection, as well as on the N.A.'s of the lenses.

Using Equations (26) or (27), along with (22), and (28), the optical transfer function for a diffuse reflector can be determined.

$$OTF = N.A._{L1}^2 \cdot T_{L1} \cdot T_{L2} \cdot N.A._{L2}^2 \cdot \rho_D \cdot O.F. \quad (29)$$

where ρ_D = reflection coefficient of a diffuse reflector and other terms are as defined in Figure 28.

In a similar manner, the OTF for the specular reflector may be determined.

$$OTF = N.A._{L1}^2 \cdot T_{L1} \cdot T_{L2} \cdot \rho_S \cdot O.F. \quad (30)$$

where ρ_S = reflectance coefficient of a specular reflector

The conclusions to be drawn here are that a specular reflector will provide a much larger received flux. However, it suffers from a coupling problem where a movement of the normal of the reflecting plane, with respect to the normal of the confocally spaced lens system, causes the incident flux upon the reflector to be reflected outside of the aperture of the receiving lens. This is shown in Figure 8.

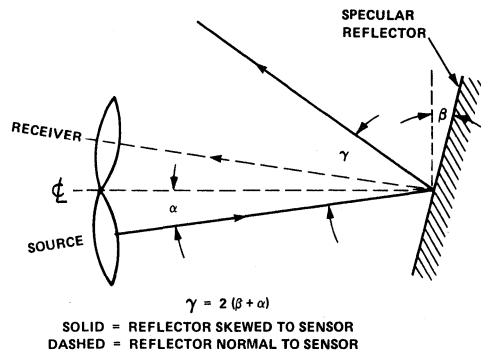


Figure 8. Positioning Sensitivity Caused by the Use of a Specular Reflecting Surface.

HEDS-1000 Reflective Coupling

Many of the alignment problems found in discrete confocally spaced reflective sensor systems can be eliminated with the use of the HEDS-1000 High Resolution Optical Reflective Sensor. This sensor includes a source and receiver focused with $2f$ optics. The optics system is a bifurcated aspheric lens with an effective numerical aperture of .3. These elements are housed in a TO-5 package with a glass window which is shown in Figure 9.

In the data sheet, radiant flux, ϕ_e , is specified as the flux coupled by the source lens to the image. This means that to develop the optical transfer function, only the receiving lens OTF need be described. The OTF for the HEDS-1000 and a diffuse reflector will appear very similar to that of a single lens system with the addition of the transmittance of the glass window, T_G , and the OTF of the reflector.

$$OTF = \frac{\phi_{RECEIVER}}{\phi_{REFLECTOR}} = T_L \cdot T_G \cdot O.F. \cdot OTF_{REFLECTOR} \quad (31)$$

The HEDS-1000 receiver area A_R is $.160\text{mm}^2$, and the source area A_S is $.023\text{mm}^2$. The ratio of A_R/A_S is greater than one which means that for focused operation, the overlap fraction O.F. is equal to one.

The following example shows the expected flux at the receiver photodiode from a diffuse reflector.

Step 1. Diffuse Reflector OTF. (32)

$$OTF = N.A._L^2 \cdot \rho_D$$

Step 2. Total OTF for HEDS-1000 Using Step 1 and Equation (31).

$$OTF = T_L \cdot T_G \cdot O.F. \cdot N.A._L^2 \cdot \rho_D$$

Step 3. Using the Following:

$$N.A._L = .3 \quad \rho_D = 98\%, \phi_e \text{ (DATA SHEET)} = 9\mu\text{W}$$

$$T_G = .9 \quad T_L = .8 \quad O.F. = 1$$

$$OTF = (.8) (.9) (1) (.3)^2 (.98) = .064$$

Step 4. $\phi_{REFLECTOR} = \phi_e$ (DATA SHEET)

$$\phi_{RECEIVER} = \phi_{REFLECTOR} (OTF)$$

$$\phi_{RECEIVER} = 576 \text{ nW}$$

If a specular reflector were used, the flux at the receiver would be the product of the transmittance of the glass and lens, the overlap fraction, O.F., and the reflectance of the specular reflector ρ_S . This is shown in Equation (33).

$$\phi_{RECEIVER} = \phi_{REFLECTOR} (T_L) (T_G) (O.F.) (\rho_S) \quad (33)$$

$$\rho_S = .95$$

$$\phi_{RECEIVER} = 9\mu\text{W} (.8) (.9) (1) (.95) = 6.16\mu\text{W}$$

Through the use of the numerical aperture of the receiver lens, it is possible to determine the Optical Transfer Function, and using this OTF, the radiant flux that appears at the receiver surface. From the responsivity of the receiver diode, the photocurrent can be estimated.

OPTICAL SENSOR PARAMETERS

Introduction

Bar code scanning, paper edge sensing, and optical tachometry applications place specific requirements on optical resolution and electrical performance of a reflective sensor system.

This section will describe the expected optical resolution and electrical performance of the HEDS-1000 as the object being sensed is placed at a location other than the optical focus point.

Modulation Transfer Function

The optical resolution of a reflective sensor system is determined by the overlap area of the images focused at the reflector surface. This may be limited by either source or receiver image size, whichever is the smaller. Optical resolution of a reflective sensor system is defined as the ability to discriminate the reflection of closely spaced lines with unequal reflectances. Figure 10 shows a series of reflectors and bars, and the response to this pattern as the imaged source and receiver, are moved laterally across the surface. The assumption is made that the reflector reflectance, $\rho_{REFLECTOR}$, is much greater than the reflectance of the bar between the reflectors. The conclusion that can be drawn from this illustration is that the ability of the sensor to discriminate between reflectors spaced a distance, s , apart increases as the space, s , increases.

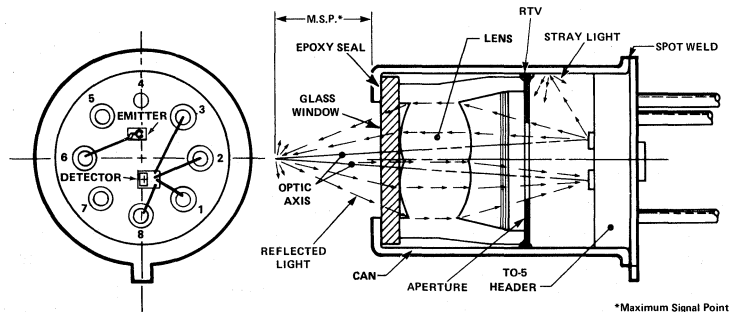


Figure 9. Elements of the HEDS-1000 High Resolution Optical Reflective Sensor.

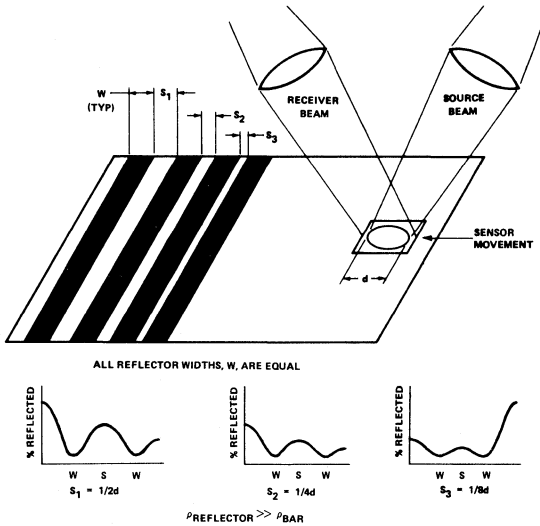


Figure 10. Resolution of an Optical Reflective Sensor System.

$$\text{Resolution} \propto \frac{s}{d} \quad (34)$$

Figure 11a, b shows a reflector object with a reflecting surface composed of equal width reflecting (white), and non-reflecting (black) lines. When a receiver with a circular image with a diameter, d , is positioned over the reflector so that the image area totally intersects the white line, a maximum or 100% peak reflected response will result. In a similar manner, when the image is positioned over the black line, a minimum or 0% peak reflected response will occur. The difference between maximum and minimum response specifies the peak amplitude response under these line width-image diameter conditions.

If this scanning spot were scanned laterally across the black-white transition, the response would be a ramp with a slope (% RESPONSE/lateral distance) determined by the image diameter. This is shown in Figure 12a. The 50% response point shown in Figure 12b indicates that the image area is equally intersecting the black-white reflecting areas. If the lateral scanning were continued across the surface, the reflected response for Figure 11a would be a trapezoidal wave form. This is shown in Figure 11b.

If an image is used to scan a black-white pattern where the line width is much smaller than the image diameter, the minimum to maximum response will be reduced from the response obtained when the line width is much larger than the image size.

An example of this is shown in Figure 13. A total 0-100% response occurs for a $W_2 = 3$ condition, while

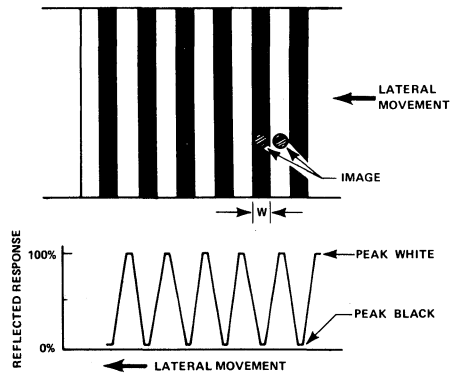


Figure 11. a,b. Image Response for Equally Spaced White and Black Lines.

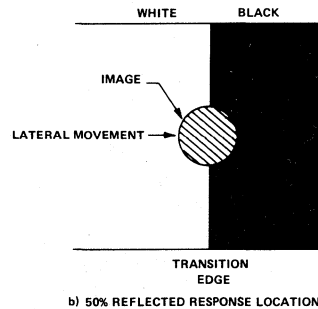
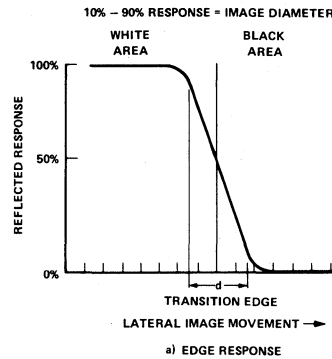


Figure 12. Image Transition Response.
a) Edge Response
b) 50% Reflected Response Location

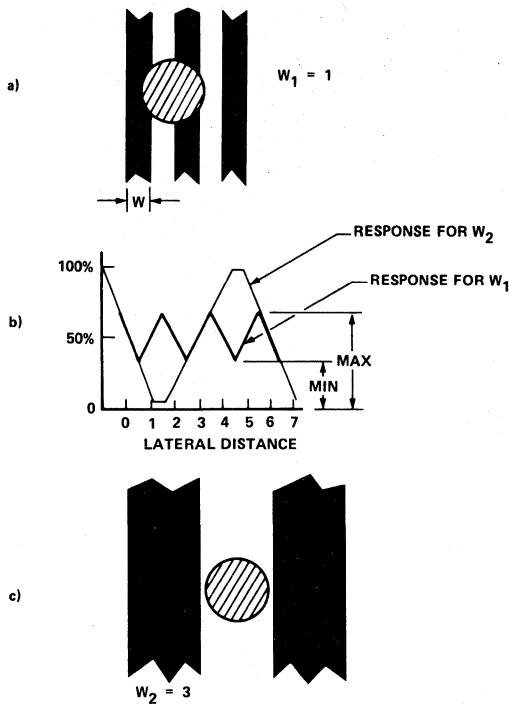


Figure 13. Reflection Modulation for Different Line Widths.

only a 33% minimum to maximum response is obtained when $W_1 = 1$. Thus, as the line width gets smaller with respect to the image, the difference between the minimum and maximum is also reduced. When the performance at smaller line widths is compared to the performance for line widths resulting in 100% response, a modulation ratio is obtained. This ratio is shown in Equation (35) using data from Figure 13.

$$\text{Modulation} = \frac{\text{MAX} - \text{MIN}}{\text{MAX} + \text{MIN}} \quad (35)$$

The modulation performance for different line pair widths for a fixed image size is called the Modulation Transfer Function, MTF, of the optical image system. The MTF is specified as a percent response at a particular spatial frequency. The spatial frequency, F , is defined as the number of equal width white-black line pairs per lateral distance. The common units for spatial frequency is line pairs per millimeter, $\ln \text{ pr/mm}$. The spatial frequency is determined by Equation (36).

$$F = \ln \text{ pr/mm} = \frac{1}{2 \text{ line width (mm)}} \quad (36)$$

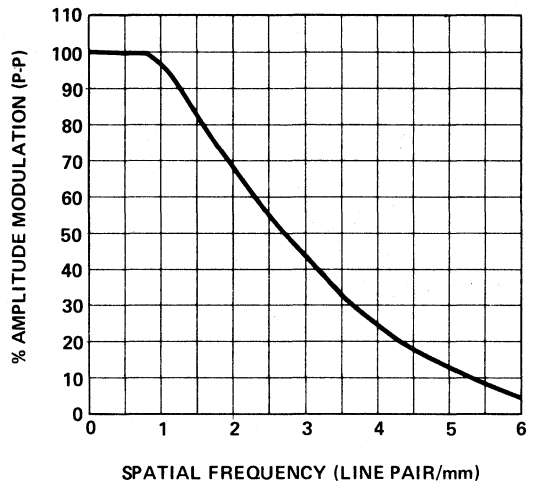


Figure 14. Modulation Transfer Function of the HEDS-1000.

Figure 14 shows the modulation transfer function, MTF, for the HEDS-1000. In applications such as bar code scanning and optical tachometry, the spatial frequency can be calculated with Equation 36. If a black-white line pattern with a line width of .254 mm (.01 in.) were to be scanned by the HEDS-1000, the performance can be determined through the use of Figure 14 and Equation (36). The spatial frequency is determined to be 1.97 $\ln \text{ pr/mm}$ which results in an MTF response of 70%.

The MTF performance indicates that when a line pattern is scanned by the HEDS-1000, the reflected flux is degraded from the amount of flux obtained from a non-patterned reflector. Thus, the MTF response becomes another element to be added to the optical transfer function, OTF, as given in Equations (32) and (33).

Depth of Field

The optical transfer function, OTF, of a reflective sensing system was presented in the Lens Reflective Coupling, and the HEDS-1000 Reflective Coupling Sections. In each case, the assumption was that the source and the received image were focused on the same plane. In most applications, the mechanical alignment of the sensor to the reflecting element will not be at the fixed focused point.

As the reflecting object moves away from the focus point, the image will become defocused resulting in a blurred image. In a reflective sensor system, the defocusing will occur for both the source and received image. The ratio of the intersection of the two image areas determines an overlap fraction, O.F.. As the system is defocused, the overlap, O.F., decreases.

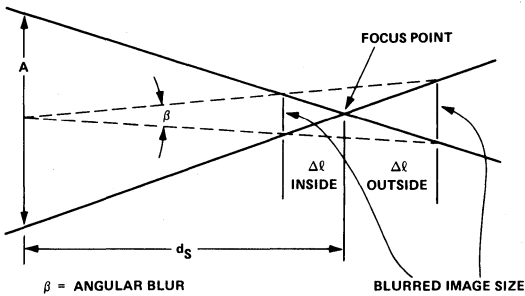


Figure 15. Defocusing Versus Depth of Field.

The defocused coupling response versus reflector distance is referred to as the depth of field, Δl . Figure 18 shows the relative response versus reflector distance. One will note an asymmetrical response on either side of the maximum signal point. There is a much sharper $\% I_P(\Delta l)$ response roll-off for the distance between the reference plane to the maximum signal point, MSP, than from the MSP, to distances further away. This is due to the fact that the amount of blurring on the near side of the MSP is less than that on the far side. This is shown in Figure 15. The blurred image at Δl inside is smaller than the blurred image at Δl outside. When a reflective type of lensed system, as shown in Figure 9, is considered, the overlap fraction, O.F., is smaller at a Δl inside than that for the same Δl outside.

The defocusing of the optical system also impacts the modulation transfer function. As the system is defocused, the image size will increase causing a reduction in the MTF for a specified line pair per millimeter.

HEDS-1000 Total Transfer Function

The optical transfer function for the HEDS-1000 was developed in the HEDS-1000 Reflective Coupling Section. This development specified the performance of the reflective sensor as a ratio of flux incident at the receiver ϕ_R to the flux ϕ_e incident at the reflector, $OTF = \phi_R / \phi_e$. The electrical designer needs to know the relationship of the current supplied to the emitter, I_F , which produces a photocurrent, I_{PR} in the detector. This relationship will be referred to as the sensor electrical transfer function or total transfer function, TTF.

The TTF is the product of the optical transfer function, the flux from the emitter, ϕ_e , and the flux responsivity, R_ϕ , of the photodiode. This is shown in Equation (37).

$$TTF = \frac{I_{PR}}{I_F} = R_\phi \cdot OTF \cdot \phi_e(I_F) \cdot K \quad (37)$$

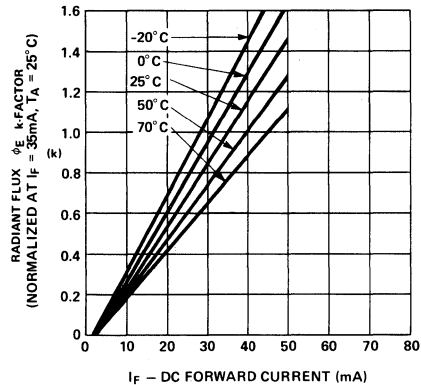


Figure 16. K-factor of ϕ_e Versus LED DC Forward Current.

The flux responsivity, R_ϕ , of the photodiode at 700 nm is specified as $.22A/W$. The flux responsivity, R_ϕ , will be considered a constant throughout the calculations. The radiant flux, ϕ_e , from the source is dependent upon the current through the LED emitter. The K-factor relationship of the output flux, ϕ_e , to LED forward current, I_F , is shown in Figure 17. This graph is normalized at 35mA and 25°C. Thus, the data sheet typical of $9\mu W$ occurs at 35 mA and 25°C.

The following example will illustrate how the TTF is used for a bar code scanner.

Given: $I_F = 45 \text{ mA}$ $\phi_e(35 \text{ mA}) = 9\mu W$
 $T_A = 25^\circ C$
 Reflector = Lambertian, $\rho_D = .85 @ 700 \text{ nm}$
 Bar Width = $.01'' = 0.254 \text{ mm}$
 Depth of Field = $\Delta l = .6 \text{ mm}$
 $N.A.L = .3$ $T_G = .9$ $T_L = .8$
 $R_\phi = .22 \text{ A/W}$

The total transfer function, TTF, is:

$$TTF = \frac{I_{PR}}{I_F} = R_\phi \cdot T_L \cdot T_G \cdot N.A.L^2 \cdot \rho_D \cdot O.F.(\Delta l) \cdot \phi_e \cdot K \quad (38)$$

The first step is to evaluate the overlap fraction, O.F. (Δl) = $\% I_{PR}(\Delta l)$, a function of the depth of field, Δl . From Figure 19, the $\% I_{PR}(\Delta l) = 50\% = .5$. Thus, the O.F. is equal to $.5$.

The second step is to determine the MTF response for a bar width of $.254 \text{ mm}$, for a depth of field of $.6 \text{ mm}$. Equation (36) is used to arrive at an $F(APP) = 1.97 \text{ ln pr/mm}$. Figure 14 is used to determine the MTF (APP) of 70%. Thus, MTF (1.97 ln pr/mm) is equal to 70%.

The third step is to determine the K-factor. This can be found from Figure 16. The K-factor for an $I_F = 45$ mA is equal to 1.3 at 25°C.

These values of O.F. ($\Delta\ell$), MTF(APP), and K are substituted into Equation (38) to determine the reflected photocurrent, I_{PR} .

$$I_{PR} = .22 \text{ A/W} \cdot .8 \cdot .9 \cdot (.3)^2 \cdot .85 \cdot .5 \cdot .7 \cdot 9\mu\text{W} \cdot 1.3$$

$$I_{PR} = 49.6 \text{ nA}$$

The conclusion that can be drawn from this example is that there are many factors contributing to the total transfer function.

HEDS-1000 Logic Interfacing

Optical sensing applications may be accomplished with the HEDS-1000 High Resolution Reflective Optical Sensor. This device includes a 700 nm emitter, a bifurcated aspheric lens, and a photodetector. The cathode of the LED emitter and the substrate of the photodetector are electrically connected to the mechanical package. The photodetector may be interconnected as a discrete photodiode or a photodiode-transistor amplifier.

Photodiode Interconnection

The photodiode, within the integrated photodetector, is isolated from the substrate-case by substrate diodes. These diodes appear from the common substrate-case to the transistor collector, and to the cathode of the photodiode.

Figure 17 shows recommended interconnection of the unused terminals of the sensor when discrete photodiode operation is desired. Care should be taken to ensure that these substrate diodes are always reverse biased so that they do not create a conductive path that may damage the substrate or other circuit elements.

The photodiode behaves like a current source, such that when optical flux falls on the device, it will generate a photocurrent in relationship to its responsivity, R_{ϕ} , of approximately $.22\mu\text{A}/\mu\text{W}$ at 700 nm. The total photocurrent, I_P , generated by this photodiode is the summation of two currents, the reflected photocurrent, I_{PR} , and a stray photocurrent, I_{PS} . Thus, $I_P = I_{PR} + I_{PS}$.

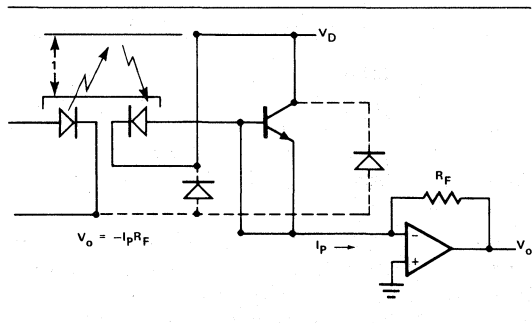


Figure 17. Photodiode Transresistance Amplifier.

Stray Photocurrent – I_{PS}

The stray photocurrent, I_{PS} , results from flux falling on the detector from sources other than the reflector surface. The principle source of stray photocurrent is from the scattered flux of the LED emitter that is reflected within the mechanical package. Ambient light can also be a source of the stray photocurrent, but this source has been greatly minimized by the use of an optical long wave filter. This filter action is provided by the red coloration found in the bifurcated lens.

$I_{PR} - I_{PS}$ Ratio

The magnitude of the stray photocurrent resulting from internal scattering is directly proportional to the forward current, I_F , through the LED and the emitter relative efficiency. DC operation of the emitter will result in a steady state stray photocurrent that will range in direct relationship to the specifications and the worst case or typical value of $I_P(\text{MIN})$ and $I_P(\text{MAX})$ related to the stray photocurrent ratio, I_{PR}/I_{PS} . The photocurrent specified for the HEDS-1000 is the total photocurrent, I_P , which is equal to the sum of I_{PR} and I_{PS} . The ratio of I_{PR} to I_{PS} is designated a quality or Q-factor of the sensor. Thus, as Q increases for a given I_P , the value of stray photocurrent, I_{PS} , decreases. A worst case analysis for I_{PS} under the condition of minimum $Q=4$, and an LED current of 35 mA results in an $I_{PS}(\text{MIN})=20$ nA for $I_P(\text{MIN})=100$ nA, and $I_{PS}(\text{MAX})=50$ nA for $I_P(\text{MAX})=250$ nA. A typical value of $Q=6.5$ would cause I_{PS} to range from 13 nA to 33 nA.

The quality factor, Q, relationship to I_P , I_{PS} , and I_{PR} is shown in Equation (39).

$$Q = \frac{I_{PR}}{I_{PS}} \quad I_P = I_{PS} + I_{PR} \quad (39)$$

$$I_{PR} = I_P [Q/(Q + 1)] \quad I_{PS} = I_P [1/(Q + 1)]$$

where Q = Quality Factor
 I_P = Total Photocurrent
 I_{PR} = Reflected Photocurrent
 I_{PS} = Stray Photocurrent

Depth of Field With Respect to Maximum Signal Point

Figure 18 shows that the 100% maximum reflected photocurrent, I_{PR} , response occurs at the location from the reference plane defined as the Maximum Signal Point, MSP. It also shows that the value of the reflected photocurrent I_{PR} is reduced as the reflector is moved in either direction away from the maximum signal point. The HEDS-1000 has a relatively symmetrical response of I_{PR} versus the distance, ℓ , from the MSP. The depth of field of this optical system is defined as the distance, $\Delta\ell$, between two equal percentage response points on either side of the MSP. The 50% I_{PR} response is referred to as the depth of field full width half maximum, FWHM. The depth of field, $\Delta\ell$, FWHM shown in Figure 18 is found to be 1.2 mm. Thus, if the

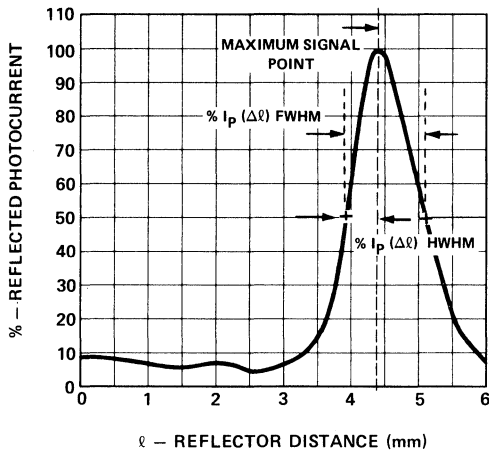


Figure 18. Depth of Field vs. Maximum Signal Point.

reflector were moved one half of the total FWHM distance, $\Delta\ell$, from the MSP, the 50% I_{PR} point would occur approximately .6mm on either side of the MSP location. The reflected photocurrent, I_{PR} , response at a specific depth of field is referred to as the % $I_{PR}(\Delta\ell)$. This value is always less than or equal to 100%.

The specific value of the I_{PR} is dependent upon the flux from the emitter and the type and reflection coefficient, ρ , of the reflector. The reflector fundamentals section presented the characteristics of the reflectors, and demonstrated that a specular reflecting surface offers and order of magnitude improvement in the reflecting photocurrent when compared to a diffuse surface.

When a diffuse reflector is used, the expected value of the reflected photocurrent, at a specific depth of field, $I_{PR}(\Delta\ell)$, is the product of the percent response of I_{PR} at the depth of field % $I_{PR}(\Delta\ell)$, the reflection coefficient, ρ , of the reflector, the total photocurrent measured at the MSP from a diffuse reflector at a specific LED current $I_P(I_F)$, and the quality ratio $Q/Q + 1$. This relationship is shown in Equation (40).

$$I_{PR}(\Delta\ell) = \%I_{PR}(\Delta\ell) \cdot \rho \cdot I_P(I_F) \cdot Q/(Q + 1) \quad (40)$$

When a specular reflector is used, an additional coefficient is introduced. The HEDS-1000 I_{PR} performance is specified for a diffuse reflector; thus, when a specular reflector is used, an improvement factor dictated by Equation (23) is obtained. This factor indicates the I_{PR} improvement, for $\rho_S = \rho_D$, is inverse of the lens numerical aperture squared. The $I_{PR}(\Delta\ell)$ response for a specular reflector is shown in Equation (41).

$$I_{PR}(\Delta\ell) = \%I_{PR}(\Delta\ell) \cdot \rho \cdot I_P(I_F) \cdot Q/(Q + 1) \cdot 1/N.A.L^2 \quad (41)$$

The expected value of $I_{PR}(\Delta\ell)$ using a diffuse reflector with a reflector having a reflectance of 75%, a total depth of field of 1.2 mm (.6 mm each way), and LED emitter current of 35 mA, and quality factor $Q = 6.5$, can be determined from Equation (40). The depth of field of 1.2 mm is equal to a 51% $I_{PR}(\Delta\ell)$ of 50%, and typical $I_P(35 \text{ mA} = 140 \text{ nA})$. The $I_{PR}(\Delta\ell)$ under these conditions is equal to 45.5 nA. If a specular reflector were used, an $I_{PR}(\Delta\ell) = 506 \text{ nA}$ would be found from Equation (41), for $N.A.L = 0.3$.

These two equations are useful in determining the expected range of I_{PR} for a given reflector and a depth of field. These two system elements are very important in bar code scanning and paper edge sensing where the type of reflector and specific depth of field are variables.

Amplifier Considerations

Each sensor application will generally specify the electrical interface required and the range of the types of reflectors which will be utilized. The magnitude of the photocurrent generated by the photodiode is normally too small to interface directly to a logic gate. This condition indicates that an amplifier is needed. The amplifier electrical performance parameters, such as current and voltage gain, and the type of coupling are determined by the logic family to be interfaced, the application, and the magnitude of the reflected photocurrent.

Applications using specular reflectors include tachometry and optical limit sensing, while diffuse reflectors are more generally found in paper edge sensing and bar code reading. An ac coupled amplifier is acceptable in tachometry and bar code reading, while a dc coupled amplifier is required for steady state applications such as paper edge sensing and optical limit sensing.

The relationship of the reflected photocurrent, I_{PR} , to stray photocurrent, I_{PS} , has a large effect on the type of dc amplifier design selected. The initial step in amplifier design is to determine the worst case magnitude of the stray photocurrent, I_{PS} . It is this worst case value of I_{PS} that becomes the input quiescent bias current, which sets the threshold for the dc amplifier output voltage.

Transresistance – TTL Interface

A very common dc amplifier used with photodiodes is the transresistance type of amplifier. The simplest form is shown in Figure 15.4.1-1. The circuit configuration described by the electrical transfer function, $V_o = -I_{PR}R_F$, is often called a current to voltage converter. A single power supply transresistance amplifier is shown in Figure 20. Here the photodiode is connected to the inverting input, and an offset voltage derived from V_{CC} is determined by a resistive voltage divider, $1 + R_2/R_1$ and is applied to the non-inverting input. The electrical transfer function is:

$$V_o = \frac{V_{CC}}{1 + R_2/R_1} - I_{PR}R_F \quad (42)$$

where $I_P = I_{PR} + I_{PS}$

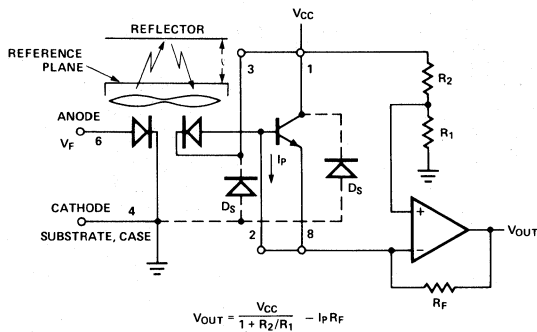


Figure 19. Photodiode Transresistance Amplifier with Offset Voltage.

Equation (43) indicates that under the condition of zero reflected photocurrent, $I_{PR}=0$, the output voltage, V_o , will be the offset voltage less the voltage developed by the stray photocurrent, I_{PS} , times the transresistance, R_F . Thus, the relationship for $I_{PR} = 0$ is:

$$V_o = \frac{V_{cc}}{1 + R_2/R_1} - I_{PS}R_F \quad (43)$$

When the transresistance amplifier shown in Figure 19 is used to interface the photodiode to a TTL logic device, the output voltage, V_o , of the amplifier must change from a logic high, V_{IH} , of 2.0V to a logic low, V_{IL} , of .8V. To improve the noise immunity of the interface, it is desirable to broaden the range of V_{IH} to V_{IL} to 2.4V and .4V. The offset voltage and the value of the transresistance resistor, R_F , is selected to insure that the maximum value of stray photocurrent, $I_{PS(MAX)} = 50$ nA, does not cause the output voltage, V_o , to fall below V_{IH} of 2.4V, and the minimum total photocurrent, $I_P(MIN) = 100$ nA, will cause the V_o to be equal to a $V_{IL} = .4V$.

It is very unlikely that an $I_{PS(MAX)} = 50$ nA and $I_P(MIN) = 100$ nA will occur simultaneously for a single device. A device that has an $I_{PS(MAX)}$ of 50 nA would also have an $I_P(MIN)$ of 250 nA. In a similar manner, a device that has an $I_P(MIN)$ of 100 nA would most likely have an $I_{PS(MAX)}$ of 20 nA.

Figure 20 shows the graphic construction of the electrical transfer function for Equation (42). The interface conditions of $[I_{PS(MAX)}, V_{IH}]$ and $[I_P(MIN), V_{IL}]$ describe a line whose y intercept dictates the offset voltage, V_{offset} , and whose slope determines the transresistance, R_F . Using Equations (44) and (45), the offset voltage, V_{offset} , and the transresistance can be determined.

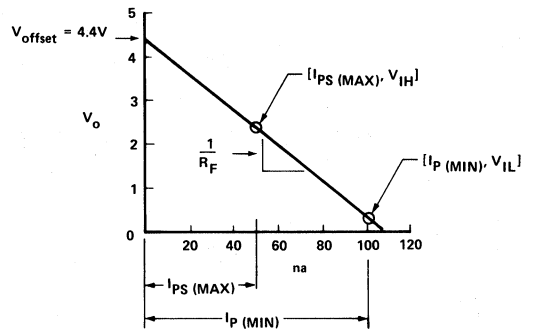


Figure 20. Graphical Solution of Transresistance Amplifier Design.

$$V_{offset} = \frac{V_{IL} I_{PS(MAX)} - V_{IH} I_P(MIN)}{I_{PS(MAX)} - I_P(MIN)} \quad (44)$$

$$R_F = - \frac{V_{IH} - V_{IL}}{I_{PS(MAX)} - I_P(MIN)} \quad (45)$$

The value of V_{offset} and R_F which satisfy the TTL interface conditions can be determined from Equations (44) and (45). For the example, $V_{offset} = 4.4V$, and $R_F = 40$ M Ω .

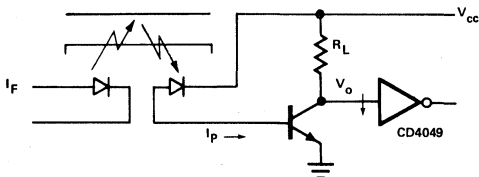
This example of photodiode-logic interfaces places parametric demands on the instrumentation operational amplifier selected. This amplifier should have a very low input offset current, thus allowing sensing of I_P at very low levels. It should have a gain greater than that required for the interface. For example, the required current gain for the photodiode-TTL amplifier is approximately 85dB; thus, an amplifier with an open loop gain of 100dB would be desirable. The slew rate of a transresistance amplifier may be slower than that required for TTL logic interconnection; thus, it may be necessary to specify a Schmitt trigger gate as the interconnecting logic element.

CMOS Interface

The internal transistor of the HEDS-1000 may also be used as a gain element in a single or multiple stage amplifier. Figure 21 shows an example of interconnecting the photodiode to a CMOS buffer gate, CD4049, using the internal transistor as a gain element.

It was shown previously that the value of I_{PS} and I_P can vary from unit to unit under similar conditions of I_F , reflector type and distance, ℓ . There will also be variations

of the h_{FE} of the transistor from unit to unit. The design of the photodiode-transistor amplifier to CMOS logic gate must take into consideration the variations of I_{PS} , I_P , and h_{FE} when a direct coupled interconnection is desired. Figure 21 presents a design for an HEDS-1000 CMOS interface. The first step is to calculate the worst case stray photocurrent, $I_{PS}(MAX)$. The $I_{PS}(MAX)$ becomes the transistor base current which, when multiplied by the $h_{FE}(MAX)$, will determine the maximum collector current resulting from stray photocurrent. It is a requirement of this circuit that the collector current resulting from $I_P(MAX)$ does not cause the collector output voltage to fall below the input logic high level, V_{IH} , of 4 volts. Thus, the maximum value of the load resistor is selected based on the $I_{PS}(MAX)$ and $h_{FE}(MAX)$ of the sensor.



CONDITIONS

$I_F = 35 \text{ mA}$

$h_{FE} = \text{MIN} = 100, \text{MAX} = 300$

$I_P = \text{MIN} = 100 \text{ nA}, \text{MAX} = 250 \text{ nA}$

$$\left[\frac{I_{PR}}{I_{PS}} \right]_{(MIN)} = Q_{(MIN)} = 4 \therefore I_{PS} = \frac{20 \text{ nA MIN}}{50 \text{ nA MAX}}$$

Figure 21. HEDS-1000 Interface to a CMOS Gate.

It is desirable in this type of interface to have at least a two to one difference between the $I_{PS}(MAX)$ and the $I_P(MIN)$. Such a stipulation will place constraints on the type of reflector, the depth of field, and the allowable spread between $h_{FE}(MIN)$ to $h_{FE}(MAX)$. Equations (40) and (41) are used to calculate the $I_P(\Delta\ell)$ for worst case conditions of $I_P(MIN)$ when a depth of field of 1.2 mm is desired. Thus, a diffuse reflector would cause 37.5 nA $I_P(MIN)$ and a specular reflector would result in an $I_P(MIN)$ of 416 nA. Using the criteria of $I_P(\Delta\ell)/I_{PS}(MAX) \geq 2$ [where $I_P(\Delta\ell)$ is evaluated for $I_P(MIN)$] indicates that a reflector with specular properties should be used.

The next step is to determine the minimum value of R_L for the minimum value of $I_P(\Delta\ell)$ and $h_{FE}(MIN)$ which causes the transistor collector voltage to fall below the V_{IL} of the CMOS gate.

This worst case analysis of Table 1 indicates that there is a very narrow range between the $R_L(MAX)$ and $R_L(MIN)$. If a smaller depth of field $\Delta\ell$ were selected, the range would be larger, thus giving a greater design margin.

Table 1. HEDS-1000 to CMOS Interface Design Procedure.

Step 1. Maximum Stray Photocurrent

$$I_{PS}(MAX) = \frac{I_P(MAX)}{Q_{MIN} + 1} = \frac{250 \text{ nA}}{4 + 1} = 50 \text{ nA}$$

$$Q_{MIN} = \frac{I_{PR}(MIN)}{I_{PS}(MAX)}$$

Step 2. $R_L(MAX)$ for V_{IH}

$$R_L(MAX) = \frac{V_{CC} - V_{IH}}{h_{FE}(MAX) \cdot I_{PS}(MAX)} = \frac{5.0 - 4.0}{300 \cdot 50 \times 10^{-9}} = 66.7k$$

Step 3. Minimum Photocurrent from Specular Reflector at $\Delta\ell = 1.2 \text{ mm}$

From Equation (41):

$$I_P(\Delta\ell) = \%I_P(\Delta\ell) \cdot \rho \cdot I_P \left[\frac{N.A.(SURFACE)}{N.A.(LENS)} \right]^2$$

$$I_P(\Delta\ell) = .5 \cdot .75 \cdot 100 \text{ nA} \left[\frac{1}{.3} \right]^2 = 416 \text{ nA}$$

$\rho = 75\%$

$N.A.(SURFACE) = 1 \quad I_P(MIN) @ I_F = 35 \text{ mA} = 100 \text{ nA}$

$N.A.(LENS) = .3 \quad \%I_P(\Delta\ell), \Delta\ell 1.2 \text{ mm} = .5$

Step 4. $R_L(MIN)$ for V_{IL} at $\Delta\ell$

$$R_L = \frac{V_{CC} - V_{IL}}{h_{FE}(MIN) \cdot I_P(\Delta\ell)} = \frac{5.0 - 2.25}{100 \times 416 \text{ nA}} = 66.1k$$

Step 5. Select $R_L = 66.2k \ 1\%$

Current Feedback Amplifier

Another common design problem is to interface the photodiode-transistor amplifier to a differential comparator such as the LM311 family. Here the design goals are similar to those specified in Figure 21 but an even greater

degree of output voltage, V_o , stability is desired. By using a simple current feedback amplifier such as the one shown in Figure 22, the variations of V_o caused by Δh_{FE} and ΔI_{PS} will be minimized. In this amplifier design, the trade-offs are between voltage/current gain, stability, and amplifier speed. As the ratio of R_F to R_L approaches unity, the V_o stability improves, but there is a loss in signal gain. The difference between the I_{PS} and $I_P(\Delta I)$ will specify a current that will cause a change in the output voltage, V_o . When a larger swing in V_o is desired, the value of R_L is increased, such that $\Delta V_o \propto (I_P - I_{PS}) R_L$. However, as R_L increases, the speed of the circuit decreases. Tables 2 and 3 show a design example using an $R_L = 100k$, $R_F = 10M\Omega$. In Figure 22, the differential comparator threshold is set by the resistor ratio R_1 , R_2 and should be equal to 1.25V. This is below the minimum quiescent, V_o , of 1.3V caused by the variations of h_{FE} and I_{PS} . The change of the quiescent voltage caused by the variation of h_{FE} can be calculated through the use of the stability factor defined as s'' . This factor is the incremental change of I_C caused by an incremental change in h_{FE} . Specifically,

$$s'' = \left(\frac{\Delta I_C}{\Delta h_{FE}} \right) \quad I_P = 0 \quad (46)$$

The V_o stability is improved as the value of s'' is reduced. The incremental V_o change of the circuit shown in Figure 22 can be calculated from the following relationship:

$$\Delta V_o = -\Delta h_{FE} \left[s'' R_L + \frac{\delta^2 V_o}{\delta h_{FE} \delta I_P} \right] \quad (47)$$

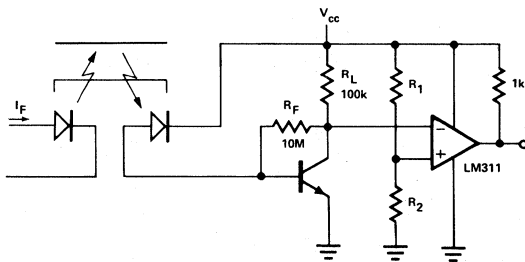


Figure 22. Current Feedback Amplifier Interface to an Analog Comparator.

Table 2 Current Feedback Amplifier Design Procedure.

OUTPUT VOLTAGE, V_o

$$V_o = \frac{V_{CC} \left(\frac{R_F}{h_{FE} R_L} \right) + V_{BE} \left(1 + \frac{1}{h_{FE}} \right) - R_F I_P}{\left(\frac{R_F}{h_{FE} R_L} \right) + \left(1 + \frac{1}{h_{FE}} \right)}$$

STABILITY FACTOR, $s'' = \frac{\Delta I_C}{\Delta h_{FE}}$

$$s'' \approx \frac{(R_L + R_F) (V_{CC} - V_{BE})}{(R_F + R_L + R_L h_{FE})^2}$$

Table 3 Practical Example of a Current Feedback Amplifier Design.

h_{FE} MIN = 100 MAX = 300 $I_{PS}(MAX) = 41$ nA
 $R_L = 100k\Omega$ $R_F = 10M\Omega$ $V_{CC} = 5.0V$, $V_{BE} = .6V$

	$h_{FE} = 100$	$h_{FE} = 300$
V_o	2.60V	1.39V
s''	1.1×10^{-7}	

The s'' parameter is important in dc coupled amplifier circuits because the change in V_o caused by the Δh_{FE} may result in the succeeding gain stages being driven into saturation.

Current-Voltage Feedback Amplifier

When even greater output voltage stability is desired, a modified current-voltage feedback amplifier may be necessary. This bias approach uses R_F and R_N as shown in Figure 23, to force a V_B which sets I_C to a level determined by V_B/R_E . This circuit can offer an s'' ten times better than the current feedback amplifier. The design is such that an h_{FE} variation of 100 – 300 will cause a 0.3V change in V_o in the current-voltage feedback configuration, while this same Δh_{FE} for Figure 22 will cause a 1.2V change.

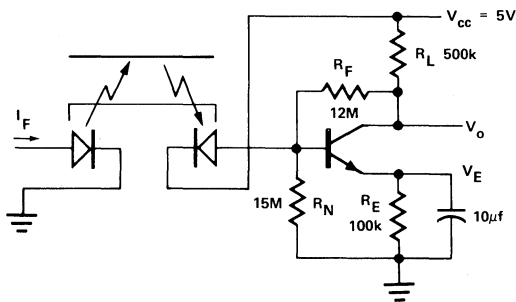


Figure 23. Current-Voltage Feedback Amplifier.

The design example given in Table 4 sets the V_o at 2.5V and offers an s'' of 7.5×10^{-9} . The output voltage V_o will be reduced from a design center of 2.5V to a worst case ($V_o - s'' \Delta h_{FE} R_L$) = 2.25V. This implies that the threshold of the comparator should be set to a level of 1.55V. This amplifier offers a transresistance of $8M\Omega$ which means for a 100 nA I_P (ΔI), the output voltage V_o will fall to 1.5V which is a sufficient differential to cause the LM311 output to change logic states.

Table 4. Design Equations for the Current-Voltage Feedback Amplifier.

Step 1. Select R_L Given: V_o and I_C

$$R_L = \frac{(V_{CC} - V_o)}{I_C} = \frac{2.5V}{5\mu A} = 500k$$

Step 2. Select R_E Given: V_E and I_E

$$R_E = \frac{V_E}{I_E} = \frac{.5}{4.91 \times 10^{-6}} = 101k \approx 100k$$

Step 3. Select R_N Given: I_N

$$R_N = \frac{V_E + V_{BE}}{I_N} = \frac{.5 + .6}{75 \text{ nA}} = 14.6M\Omega \approx 15M\Omega$$

Step 4. Select R_F Given: I_N and I_B

$$R_F = \frac{V_o - V_E - V_{BE}}{I_N + I_B} = \frac{2.5 - .5 - .6}{75 \text{ nA} + 50 \text{ nA}}$$

$$= 11.2M\Omega \approx 12M\Omega$$

Step 5. Stability Factor, s''

$$s'' = \frac{[V_{CC} - V_{BE} \left(1 + \frac{R_F + R_L}{R_N}\right)](g + 1)}{R_F [1 + (1 + h_{FE})g]^2}$$

$$\text{where } g = \frac{R_E}{R_N} \left(1 + \frac{R_L}{R_F}\right) + \frac{R_E + R_L}{R_F}$$

$$s'' = 7.5 \times 10^{-9}$$

LSTTL Interface

The previous circuits dealt with CMOS and comparator type interfaces. Figure 24 shows a two transistor amplifier to LSTTL interface. This circuit can either be ac or dc coupled, only the direct coupled configuration will be presented. The design approach is similar to that of Figure 21 with the additional analysis of the second stage.

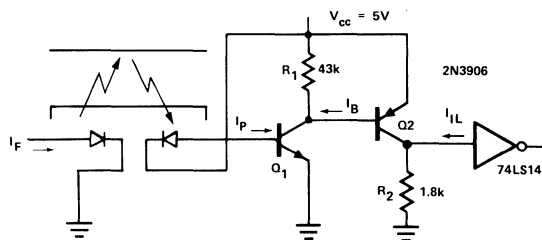


Figure 24. DC Coupled HEDS-1000 to LSTTL Interface.

The first transistor, Q_1 , is biased by the photodiode in a common emitter configuration. Under the conditions of $I_{PS}(\text{MAX})$, the collector of Q_1 is pulled up to within .5V of V_{CC} , thus insuring that Q_2 is not conducting. This condition sets the maximum value of R_1 . When a reflected

photocurrent is present, the resulting I_C of Q_1 is the combination of current through R_1 and the I_B of Q_2 . Thus, R_1 must be large enough that the current sinking capability of Q_1 (dictated by h_{FE} and I_P) will result in sufficient I_B in Q_2 to cause Q_2 to saturate.

In the absence of reflected photocurrent, both Q_1 and Q_2 are normally off. Under this condition, the load resistor, R_2 , must be able to sink the I_{IL} of the LSTTL gate at the desired V_{IL} . To satisfy the desired logic condition, R_2 must be less than V_{IL}/I_{IL} . The minimum value of R_2 is determined by the current sourcing capability of Q_2 produced by I_B . The collector current of Q_2 must generate a voltage drop across R_2 greater than the V_{IH} of the gate. It is recommended that a high gain, low leakage PNP transistor, such as a 2N3906, be selected for Q_2 .

The rate at which the output voltage of Q_2 changes is directly related to the speed at which the reflecting surface is moving into the reflection plane of the sensor. In many applications, the rate of change of V_o through the switching region of the LS gate is so slow that it may cause logic level chatter at the output of the gate. If this chatter is observed, it is recommended that a Schmitt trigger gate, such as the 74LS14, be used.

REFLECTIVE SENSOR APPLICATIONS

Rotary Tachometry

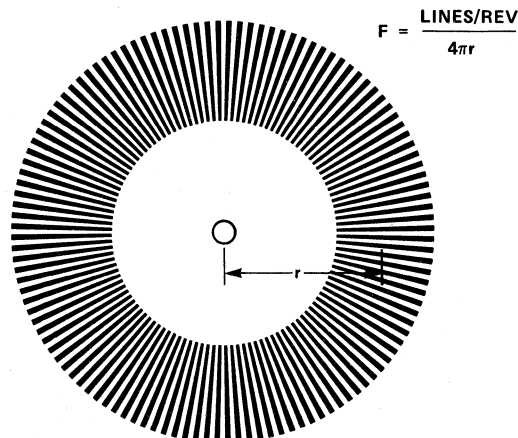
A reflective sensor can be used as the transducer to determine the rotary speed of a motor shaft. This can be accomplished by utilizing a disc with equally spaced

reflective and non-reflective lines placed around the circumference of the disc. The number of line pairs per revolution will then give a specific pulse count per revolution. In many applications, it is desired to have a very high density of line pairs around the perimeter of a small diameter disc. The performance of the reflective sensor is determined by the MTF for the spatial frequency, F , of line pairs on the disc. The spatial frequency for a disc is determined by Equation (48).

$$F = \frac{\text{lines/rev.}}{4\pi r} \quad (48)$$

Using Figure 25, the spatial frequency can be determined assuming the radius is to the center point of the line pattern. Given the radius, $r = 10$ mm, and 220 lines/revolution, a spatial frequency of 1.75 ln pr/mm is calculated. When an HEDS-1000 is used as the sensor for this code wheel, an MTF response of 75% is obtained from Figure 14.

The code wheel is affixed to a hub which is placed on the rotating shaft. The reflective sensor is positioned perpendicular to the disc and at a distance such that the maximum signal point, MSP, is at the plane of the code pattern. The highest reflected photocurrent, I_{PR} , is obtained from a specular reflecting code pattern. This can be implemented by photolithographing a pattern of opaque bars on a shiny metallic wheel-hub assembly. A diffuse code wheel assembly should be used when the mechanical tolerance of the axial alignment of the HEDS-1000 to the normal of the code wheel exceeds 10° .



SPATIAL FREQUENCY OF CODE WHEEL

Figure 25. Spatial Frequency of a Code Wheel.

Tachometry applications allow an ac coupled amplifier to be used, such as the current feedback type in Figure 22. AC coupling the output of the HEDS-1000 eliminates the dc output offset voltage variations caused by the stray photocurrent.

HEDS-1000 Analog Tachometer

The HEDS-1000 can be used as the transducer in high speed rotary tachometry applications. Figure 26 shows a circuit diagram that uses the reflective sensor as a pulse source input to a frequency to voltage converter.

The HEDS-1000 is configured as a current feedback amplifier and ac coupled to an LM2907 frequency to voltage converter. The transistor Q_1 is used as a current source to supply the I_F to the LED emitter.

The reflective sensor generates n pulses per revolution, where n is the number of line pairs per revolution. The magnitude of the frequency, f , applied to the F-V converter is n times the number of revolutions per minute. This is the relationship shown in Equation (49).

$$n = \frac{\pi r}{\text{line width}} = \frac{2\pi r}{\ln \text{pr width}} \quad (49)$$

$$f = n \text{ rev/min} \times \frac{1 \text{ min}}{60} = \frac{\text{Hz}}{\text{sec}} \quad \text{where } f = \text{Hz}$$

The capacitor, C , is the dominant factor in determining the maximum output voltage for a required full scale frequency indication. The capacitor required to determine a full scale output voltage for a specific full scale frequency is shown in Equation (50).

$$C = \frac{V_{\text{OUT FULL SCALE}}}{R \cdot V_{\text{CC}} \cdot f_{\text{FULL SCALE}}} \quad (50)$$

A $V_{\text{OUT FULL SCALE}} = 1\text{V}$, 0–25,000 rev/min tachometer can be designed using a code wheel with a radius of 20 mm and a line width of .63 mm. The approach is to determine maximum full scale frequency from Equation (49), and then using Equation (50), the full scale frequency

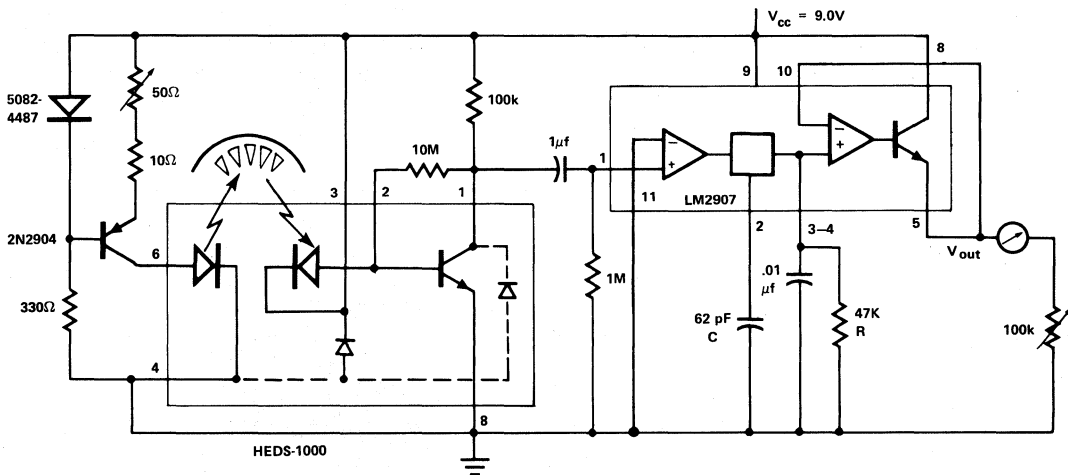


Figure 26. Analog Tachometer Circuit.

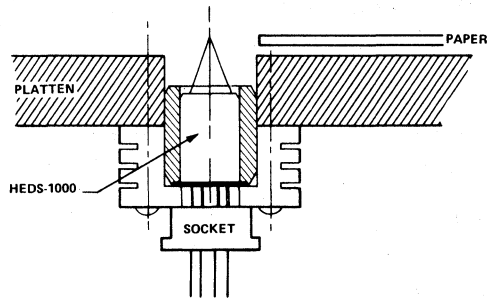


Figure 27. Reflective Type Paper Edge Sensor.

is 41.5kHz and C is calculated to be 57pF. A 62pF capacitor is used for this example.

The F-V converter will respond to a minimum input signal swing of 250mV. This input level can be insured through the use of a specular reflector. In the HEDS-1000 Total Transfer Function Section it was shown that the I_{PR} increases by 10.45dB when a specular reflector is used over a diffuse reflector. The limitation of a specular reflecting code wheel is that the HEDS-1000 alignment to the code wheel must not be greater than 10° from the normal. If the deviation is greater than 10° the image of the source will not be reflected to the detector.

Paper Edge Sensor

The accurate detection of the edge of a piece of paper can be accomplished with an HEDS-1000 reflective sensor. If the range of reflectivity of the paper is known, either a paper reflective or an obscuration system can be selected.

When a paper type which is highly reflective is considered, it is desirable to utilize a reflective system of the type that positions the sensor so that the maximum signal point lies at the surface of the paper platten. This approach is shown in Figure 27. When a low reflectance paper type is being sensed, the obscuration type system may be more suitable. Such a system is shown in Figure 28.

The edge position sensing accuracy is dependent on the spot location as referenced to the mechanical system. The HEDS-1000 offers a reflective sensing spot location of $\pm .51$ mm with respect to the package center line.

When an obscuration sensor system is used, the two transistor amplifiers shown in Figure 24 provide a convenient dc coupling to a 74LS logic family. When the reflective system is applied, a transresistance amplifier of the type shown in Figure 19 should be considered.

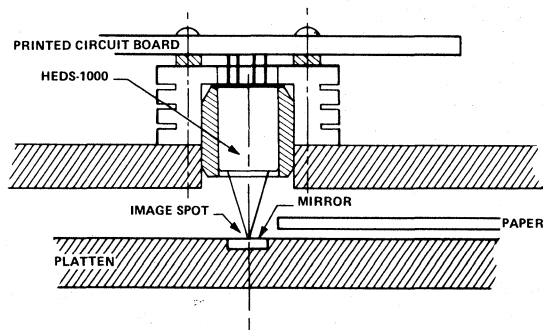


Figure 28. Obscuration Type Paper Edge Sensor.

Bar Code Scanner

A reflective optical sensor can be used as the transducer in a bar code scanner application. The bar code is an encoded form of binary data storage. The relative width difference bar to bar, and space to space, describe the typical encoding scheme of Differential Width encoding. This is the data format used in the Universal Product Code, UPC.

The sensor provides an electrical output signal with a pulse width determined by the bar and space widths, and signal amplitude dependent upon the bar and space reflection coefficients.

The Differential Width encoding scheme requires that output pulse width, bar to bar, or space to space, be an accurate representation of the distance per unit time. The accuracy of the scanning output improves when the reflecting spot size is smaller than the minimum bar or space width. The smaller the scanning image, the more abrupt the transition from bar to space.

The output signal amplitude is determined by the difference between the bar reflectance and space reflectance. The minimum output signal to maximum output signal ratio is directly proportional to the bar to space reflectance.

The signal amplifier that is interconnected to the sensor must have a large dynamic operating range to accommodate the variations of reflector types, and also provide adequate signal differential for the bar to space reflectivity difference.

Figure 13 shows the trapezoidal pulse train that is obtained from scanning a bar code of equal width bars and spaces. As the image size increases due to defocusing, the pulse train amplitude is reduced and the waveform becomes triangular. It is desirable that the amplifier provides the signal amplitude change at the same scanning location as the bar to space transition.

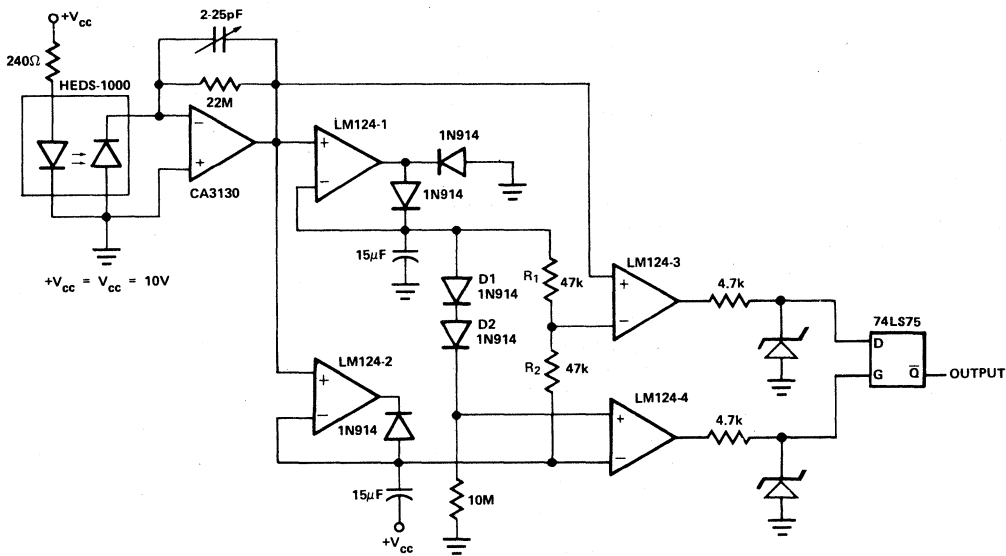


Figure 29. Bar Code Scanner Circuit.

Figure 29 shows a schematic for an amplifier system that will convert the bar and space widths into TTL compatible logic signals. The circuit uses the CA3130 as a transresistance amplifier for the HEDS-1000 photodiode. The output of the amplifier is applied to positive peak (LM124-1) and negative peak (LM124-2) detectors. The resistors R_1 and R_2 set the reference (negative-going) input to the code comparator (LM124-3) at a voltage which is halfway between the positive peak and the negative peak, so the switching threshold is therefore at

50% of the peak-to-peak modulation. The noise gate (LM124-4) compares the negative peak to a voltage which is two diode voltage drops (D_1 and D_2) below the positive peak, so unless the peak-to-peak amplitude exceeds two diode drops, the G input of the 74LS75 remains low and \bar{Q} cannot change. This ensures that the \bar{Q} output of the 74LS75 will remain fixed unless the excursions at the output of the CA3130 are of adequate amplitude (two diode drops) that noise will not interfere.